Theor. Appl. Climatol. 58, 129–139 (1997)

Theoretical and Applied Climatology

[1] Department of Agonomy, Purdue University, W. Lafayette, IN, U.S.A.
[2] USDA Forest Service, Northeastern Forest Experiment Station, Syracuse, NY, U.S.A.

Ultraviolet Sky Radiance Distributions of Translucent Overcast Skies

R. H. Grant[1], **G. M. Heisler**[2], and **W. Gao**[1]

With 6 Figures

Received August 5, 1996
Revised October 21, 1996

Summary

The diffuse sky radiation component in the ultraviolet wavelengths is often at least 50% of the global irradiance under clear skies, and is the dominant component of ultraviolet global radiation under translucent overcast skies. The distribution of sky radiance was measured in a rural area and modeled for wavelength bands of ultraviolet-B (UVB, 280–320 nm) and ultraviolet-A (UVA, 320–400 nm). Sky radiance measurements were made during the summer of 1993 over a wide range of solar zenith angles using radiance sensors mounted on a hand-operated hemispherical rotation mount. UVB irradiance measurements were also made during each scan. Since the ratio of measured irradiance under overcast skies and that predicted for clear skies was not correlated with cloud base height, opaque cloud fraction, or solar zenith angle, it was concluded that the scattering from the clouds dominated the global irradiance, and this scattering was relatively unaffected by the scattering off opaque clouds in the translucent atmosphere.

Analysis of the translucent overcast sky UVA and UVB radiance measurements using a semi-empirical distribution model showed that the spectral influences on multiple scattering, single scattering, and horizon brightening components of the distributions agreed with basic atmospheric radiation theory. The best model used solar zenith, the sky zenith, and the scattering angle with resultant coefficient of determination values of 0.62 and 0.25 for the UVA and UVB respectively. The developed equations can be applied directly to the diffuse sky irradiance on the horizontal to provide radiance distributions for the sky.

1. Introduction

The recorded decreases in stratospheric ozone at all latitudes of the earth and the measured increases in ultraviolet radiation at some locations (Madronich and DeGruijl, 1994) has increased the interest in understanding the distribution in time and space of solar ultraviolet (UV) radiation (Nunez et al., 1994). Ultraviolet radiation in the wavelength bands of 280–320 nm and 320–400 nm are termed UVB and UVA radiation and together typically comprise about 3% of the total solar radiation reaching the earth's surface. The UVB portion is less than 1% of the total. Although the amount of radiation received at the earth's surface is relatively small, the photons at these wavelengths are highly energetic and detrimental to health of plants and animals. As a result, understanding the amount of UV radiation received by plant and animal organisms near the earth's surface is important to a wide range of disciplines: tropospheric chemistry, cancer research, forestry, agriculture, ophthalmology, and oceanography.

Ultraviolet solar radiation at the earth's surface has two primary 'streams' of incoming radition: direct beam and diffuse sky. The diffuse sky

radiation is in part a function of the scattering of beam and sky radiation from the earth's surface, in part due to scattering by molecules and aerosols in the atmosphere, and in part due to scattering and transmission through clouds in the atmosphere. While our understanding of the direct beam UV radiation reaching the earth's surface is generally adequate for most studies, our understanding of the diffuse sky UV radiation is still inadequate. The understanding of the diffuse sky radiation is particularly important to estimating biological impacts of increases in UVB radiation, since the diffuse to direct ratio in the UVB is commonly greater than one for clear skies as well as cloudy skies (Garrison et al., 1978; Beaglehole and Carter, 1992). The relatively great importance of the diffuse sky UVB and the presence of many UV sensitive organisms in environments that are partially-sheltered from the sky predicates the need for a function to describe the distribution of the sky radiance for variable cloud cover. Analytical approximations of the UVB radiation have been developed for clear skies that are fundamentally two-stream models (Green et al., 1974; Green et al., 1980; Schippnick and Green, 1984). These two-stream models however provide the sky diffuse irradiance as a bulk quantity. Measurements of the diffuse sky radiance distribution shows that the sky radiance is not uniformly distributed through the sky hemisphere (Grant et al., 1996a, b; Brunger and Hooper, 1991; Coombes and Harrison, 1988). Sky radiance distributions of cloudy skies can be derived theoretically as scattering through equivalent homogeneous sheets of cloud (Stamnes et al., 1991; Nack and Green, 1974) or as fractional unobstructed and cloud obstructed direct beam (Rosen, 1992).

Clouds have similar UV scattering thicknesses as the clear sky (Spinhirn and Green, 1978) resulting in less difference in the UV sky radiance with or without clouds than found in the broadband short wave (SW) waveband. There are, to the knowledge of the authors, no sky radiance distribution functions for radiation in UV wavelength bands under cloudy skies. This paper reports on the development of sky radiance distribution functions for overcast skies consisting of translucent cloud sheets of stratus, cirrostratus, and stratocumulus with or without completely opaque but partial cloud decks of cumulus and stratus.

2. Methods

Sky radiance measurements in the UVA and UVB were made under varying sky conditions during the summer of 1993 at the Purdue Agronomy Research Center located in West Lafayette, IN, USA (40.5° N latitude). The surface UVA and UVB albedo was estimated at 2 to 5% based on the agricultural land use of the area (Blumthaler and Ambach, 1988). The local atmosphere is considered to be a "clean continental atmosphere".

Sky radiance measurements were made using silicon photodiode (SED033) and vacuum silicon photodiode (SED240) sensors produced by International Light (IL), Inc. (Newburyport, MA). The UVB radiance was measured using a sensor with interference filters while the UVA radiance was measured using a sensor with a color absorption filter. Since the spectral irradiance of solar radiation increases rapidly with increasing wavelength through the UVB wavelength band, an overall response of the sensor and filter in sunlight is a more accurate indication of the bandwidths of the sensor/filter combinations used to measure sky radiance (Fig. 1). The distribution of solar radiation in the UVA wavelength band is more evenly distributed than in the UVB, resulting in little difference between the char-

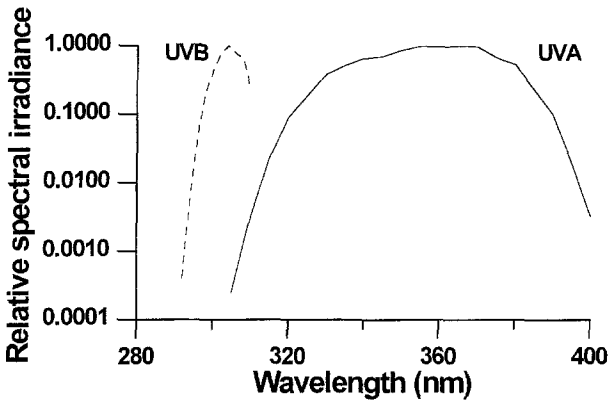

Fig. 1. Spectral response of the sensors. The relative sensor response of the UVA and UVB sensors are indicated as convolutions of the sensor response on the modeled clear-sky solar irradiance for 40° solar zenith at sea level with 0.32 Atm-cm of ozone, and a low rural aerosol load (Schippnick and Green, 1988)

acteristic response bandwidth and the actual bandwidth experienced under solar radiation. The temperatue coefficient of the SED240 and SED033 sensors was measured in the laboratory at 0.5% and 0.1% respectively (Grant, 1996). The field of view of the UVA and UVB sensors was measured at 16° (95% cutoff) (Grant et al., 1996a).

The sensor/filter/hood combinations for the UVA and UVB wavelength bands were factory calibrated in February 1993 and November 1992 respectively. The UVA sensor/filter/hood response was 5.77×10^{-4} A/W cm^{-2} Sr for monochromatic radiance at 360 nm. The UVB sensor/filter/hood response was 1.39×10^{-4} A/W cm^{-2} Sr for monochromatic radiance at 297 nm and a reverse bias on the detector.

The radiance sensors were mounted on a platform that provided for rotational and inclinational motion, similar to that reported in Grant et al. (1996a). Alignment of the radiance sensors on the platform was estimated at approximately 2°. The hemispherical distribution of the sky radiance was measured by inclining and rotating the platform. Measurements were made at approximately 10° increments in zenith from 0 to 80° and approximately 3° increments through the full 360° azimuth. The position of the platform in polar coordinates was determined by excitation of potentiometers attached to the rotating axes of the platform. The positional error for the sensors was measured to be 5° in both azimuth and zenith. Therefore the overall error in the positional information associated with each radiance measurement was approximately 7°.

Sky radiance measurements were then corrected for photodiode dark current and the temperature coefficient. Measurements of the radiance within scattering angles between the sensor measurement direction and the computed location of the solar disk of less than 15° (7° positional error and 8° field of view half width) frequently saturated the signal conditioning circuits and had to be excluded from further analysis. Therefore this region, termed the solar aureole (which according to Deepak (1977) extends approximately 20° from the solar disk), was not well described by the measurements and was excluded from this analysis. Similar exclusions of the aureole region in developing a sky radiance distribution function have been made by Coombes and Harrison (1988), Steven and Unsworth (1980), and Brunger and Hooper (1991, 1993).

UVB irradiance measurements were made during each sky scan using a SED240 sensor with UVB filter and quartz diffuser as in Grant (1996). The UVB irradiance sensor had identical temperature and spectral response characteristics as the UVB radiance sensor. UVB irradiance measurements were corrected for temperature and cosine response of the sensor (Grant, 1996) prior to analysis. The UVB irradiance and radiance measurements and radiance sensor orientation were sampled by a CR7X datalogger (Campbell Scientific, Logan UT) at two second intervals.

2.1 Normalization of the Radiance Distributions

Normalization of the sky radiance measurements was identical to that used in Grant et al. (1996a). Each set of measured sky radiance was averaged by 10° azimuth and zenith angle increments and the standard deviation from the mean for each "zone" was determined. The averaged sky radiance distributions for each zenith-angle zone of the sky ($N_a(\Theta)$ in units of W m^{-2} Sr^{-1}) were then normalized (N_m in units of πSr^{-1}) by dividing the values of $N_a(\Theta)$ by the integrated radiance I_{diff} according to:

$$\hat{I}_{\text{diff}} = 2\pi \int_0^{\pi/2} \overline{N_a}(\Theta) \cos(\Theta) \sin(\Theta) d\Theta. \qquad (1)$$

with Θ the sky zenith angle (Fig. 2). This normalization procedure reduces the influence of turbidity on the radiance distributions (Steven and Unsworth, 1980), and is similar to that used by Brunger and Hooper (1993) and Steven and Unsworth (1980). It differs from that used by Coombes and Harrison (1988); comparison of the results of this study to those of Coombes and Harrison requires a multiplication of their normalized radiance and regression coefficients by $1/\pi$. This adjustment has been made to their coefficients presented in Table 2. The normalization used in this study results in a normalized radiance equal to $1/\pi$ for the uniform overcast sky (UOC).

Measurements were excluded from the initial integration of N_a to calculate $\hat{I}_{\text{diff}}$ and all sub-

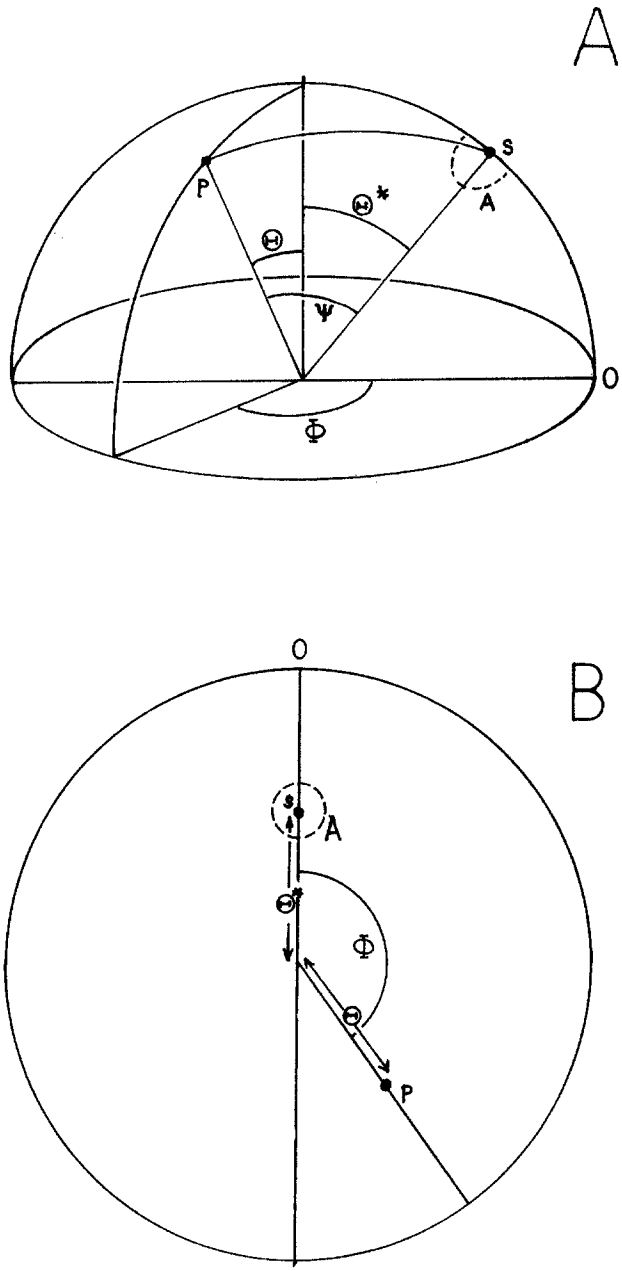

Fig. 2. Geometrical relationships of the atmospheric scattering. The sun's disk and sky location for a given radiance value are indicated by an 'S' and 'P' respectively. The solar aureole is indicated by an 'A'. The zenith and azimuth of the sun and sky location correspond with symbols used in the text. Panel A provides a perspective view of the sky hemisphere dome while panel B provides a planar map of the dome corresponding to the sky radiance maps presented in Fig. 4. Distances from the center of Panel B are linearly related to the zenith angle. (modified from Grant et al., 1996a)

sequent analysis if: 1) the scatter angle between the solar disk and the location in the sky (Ψ; Fig. 2) was less than 15°, or 2) N_a was based on less than 5 measurements. It was assumed that the diffuse sky radiance within the area of $\Psi <= 15°$ (the aureole) was predominantly governed by the same scattering physics as that further from the solar disk and that the sky radiance distribution function derived from measurements outside $\Psi = 15°$ were representative on N_a within $\Psi = 15°$.

2.2 Sky Condition Determination

Cloudy sky transmittance was estimated by the ratio between an estimated clear sky irradiance ($\hat{I}_{\text{clear}}$) and the measured obscured overcast irradiance (I_{ovc}). Clear sky UVB irradiances for solar zenith angles corresponding to the individual overcast sky scans were estimated from regressions of clear sky irradiance measured (but not published) at the time of the clear sky UV radiance measurements reported in Grant et al. (1996a). The overcast to clear sky irradiance ratio ($\overline{I_{\text{ovc}}}/\hat{I}_{\text{clear}}$) was then calculated by dividing the mean measured overcast sky irradiance $\overline{I_{ovc}}$ for each scan period by the predicted clear sky irradiance $\hat{I}_{\text{clear}}$ according to the solar zenith angle and the clear sky regression equation. The cloud UVB optical depth (including influences of cloud scattering and extinction) was estimated based on an analytical representation of the simplified theory of Nack and Green (1974) as:

$$\tau_{\text{cloud}} = \left(0.96 - 3.6 \ln\left[\frac{\overline{I_{\text{ovc}}}}{\hat{I}_{\text{clear}}}\right]\right)^2 \qquad (2)$$

assuming a center wavelength of the UVB measurement of 305 nm.

Hemispherical (180° FOV) photographs of the sky were taken before and after each complete scan of the sky. The developed slides were then projected onto a polar grid and analyzed according to the methodologies described in Grant et al. (1996a). The pool of sky hemispherical scans of all sky conditions were subdivided into classes by solar zenith angle and total cloud cover prior to normalization of the radiance and subsequent modeling of the normalized radiance distributions. Only scans taken when the total cloud cover was recorded as 9 or 10/10ths by the National Weather Service (NOAA) observer at the Purdue University Airport (approximately 15 km away) and the photographic analysis resulted in a cloud cover of greater than 90%

Table 1. *Atmospheric Conditions During Sky Scans Used in the Analysis*

	Overcast (ovc) skies			Clear (clr) skies[1]			
Θ^* Range (Deg.)	Mean Θ^* (Deg.)	UVB τ_{cloud}	n^2	Mean Θ^* (Deg.)	Mean τ_a^4	n	Mean UVB $\overline{I_{ovc}}/\hat{I}_{cir}$
25–34.9	29.0	10.0	24	29.2	0.339	14	0.66
35–44.9	39.1	9.5	20	39.7	0.371	15	0.70
45–54.9	48.5	6.0	18	48.2	0.317	13	0.82

Θ^* = solar zenith angle
n = number of replicate samples
[1] values from Grant et al. (1996a)
τ_a is the aerosol turbidity determined by the Langley method

were used in this analysis. If overcast conditions existed, then the visibility of the solar disk was determined from the photographic slides and only scans in which the solar disk was visible were included in the database (Table 1). Cloud type was also assessed by viewing of the photographic slides in combination with the cloud layer base heights reported by the observer at the Purdue University Airport. The opaque cloud cover fraction (that part of the sky in which no blue hue was evident above the cloud) for the translucent overcast skies, also measured by the observer at the Purdue University Airport, was correlated to $\overline{I_{ovc}}/\hat{I}_{clear}$.

2.3 Radiance Models

Two overcast sky radiance functions were evaluated in combination with the previously developed clear sky radiance functions for their utility in describing the normalized UVB and UVA sky radiance under overcast skies. The resultant normalized sky radiance distributions were fit to published sky radiance distribution functions and the coefficients of the fit compared to those determined for SW radiation.

The overcast sky radiance distribution function derived by Coombes and Harrison (1988) for the SW radiance was of the form:

$$N(\Theta, \Theta^*, \Psi) = A + B\Theta^* + C\cos\Theta + De^{-m\Psi} \tag{3a}$$

where the first two terms describe the isotropic multi-scattering component, the third term represents the horizon darkening, and the last term represents the single scattering circumsolar component, the solar zenith angle is Θ^*, and Ψ is the scattering angle defined as:

$$\cos\Psi = \cos\Theta\cos\Theta^* + \sin\Theta\sin\Theta^*\cos\Phi \tag{3b}$$

A complete description of the angles used in the analysis are illustrated in Fig. 2. Multiple scattering in the atmosphere was evaluated based on the values of the first two terms in Eq. (3a) when $\Theta^* = 30°$. This formulation was also used successfully by Grant et al. (1996b) to describe the photosynthetically active radiation (PAR) radiance distribution for translucent overcast skies.

The second overcast sky radiance distribution function, initially developed by Powkrowski (1929) and used by Steven and Unsworth (1980) to describe the overcast sky radiance distribution in the SW waveband, was the Standard Overcast (SOC) type sky radiance function:

$$N(\Theta) = N(0)\left[\frac{1 + b\cos(\Theta)}{1 + b}\right] \tag{4}$$

where $N(0)$ is the normalized radiance at the Zenith. The SOC is often assumed to be a good estimate of the overcast sky conditions for sky luminance (Fritz, 1955) and the total short-wave (SW) waveband radiance (Steven and Unsworth, 1980). The model however could not be fit to results of SW radiance measurements by Coombes and Harrison (1988) and PAR radiance measurements (Grant et al., 1996b). Recent efforts by Kittler and Valko (1993) and Grant

et al. (1996b) have shown that the SOC sky distribution works well only when the solar disk is entirely obscured.

The non-linear regression procedure used a sequential least square error fitting routine (Draper and Smith, 1981) while constraining the solution such that:

$$\int_0^{2\pi}\int_0^{\pi/2} N(\Theta,\Phi)\cos(\Theta)\sin(\Theta)d\Theta d\Phi = 1. \quad (5)$$

All angles represented in the various equations described above were in units of radians. The goodness of fit of the averaged and normalized sky radiance to a model radiance distribution was determined by minimizing the root mean squared error (RMSE) between the actual measurement and the modeled radiance (Grant et al., 1996a, b).

In non-linear regression, there are commonly more than one solution (Draper and Smith, 1981). The initial values for the coefficients were set to either 0.1 or the values determined for the total short-wave radiation (Table 2). Passes of the nonlinear fitting routine were conducted until the RMSE varied by less than 0.5%. It was assumed that the small improvement indicated that the solution to the equation was stable.

Variability in the UVB radiance measurements resulted in some extreme values that are believed to be due to electrical noise induced on low signals which typically occurred near the horizon and in the entire sky hemisphere during measurements at the highest solar zenith angles. As a result, model residuals were highly skewed for the UVB. Further qualification of the data was made using a skewness test for outliers (ASTM, 1980) applied to the model residuals. Mathematically, the test statistic compared the skewness of the residual values to that based on the theory of random sampling of a normal distribution as developed by Ferguson (1961).

3. Results and Discussion

The translucent overcast sky conditions had UVB irradiance levels between 68 and 82% of that for the clear sky conditions at the same solar zenith angle. This is reasonable in comparison to the irradiance ratio of optically thin overcast sky conditions at high elevation of 0.70 (Blumthaler et al., 1994). It is important to realize that translucent overcast skies consist of cloud layers distributed in a way that the solar disk was visible during the measurement period, but that fractions of the sky may have opaque clouds that if between the sun and observer would result in obscuration of the solar disk. Cloud types discernible by the slide photographs varied from single or multiple layers of translucent cirrostratus, cirrus, altostratus, or altocumulus in combination with opaque clouds such as cumulus and stratocumulus. The opaque cloud cover did not however correlate with the irradiance ratio (Fig. 3A). Values of the irradiance ratio greater than one are probably due to different aerosol and ozone column conditions between the clear sky scans reported in Grant et al. (1996a) and the translucent overcast sky scans reported here, and not enhanced radiance in the UV due to scattering off clouds suggested by Nack and Green (1974) since the ratio is established based on a

Table 2. *Overcast Sky Radiance Distribution Functions*

	Equation coefficients					
Wavelength band	A	B	C	D	m	RMSE[1] (πSr^{-1})
Translucent overcast						
SW[2]	0.143	0.357	0.137	0.229	1.88	
PAR[3]	0.074	0.059	0	0.546	1.8	
UVA n = 791	0.120	0.032	0.064	0.361	1.9	0.031
UVB n = 496	0.152	0.029	0.029	0.247	1.7	0.091

[1] Root mean squared error
[2] Coefficients after division by π from Coombes and Harrison, 1988
[3] Corrected coefficients from combined OVC PAR radiance of Grant et al., 1996b

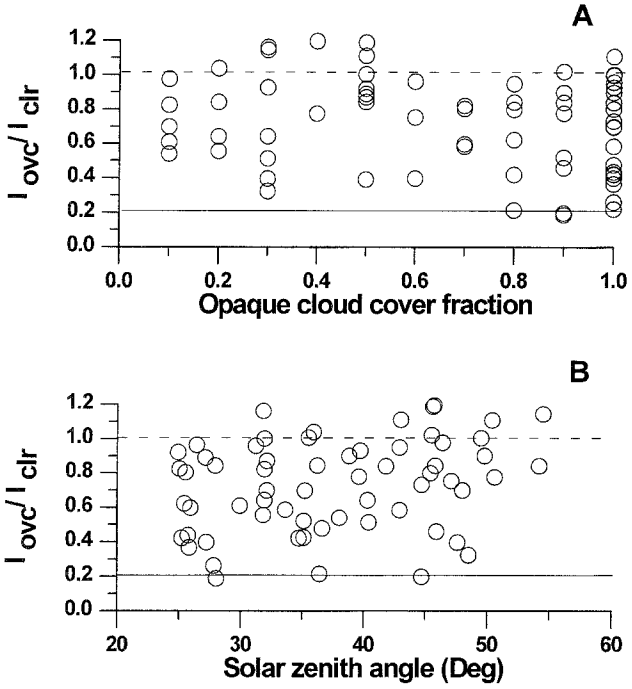

Fig. 3. UVB Irradiance ratios for the translucent overcast skies. The irradiance ratios for translucent overcast sky conditions are shown relative to opaque cloud fraction (panel A) and solar zenith angle (panel B). The dashed line is the nominal irradiance for clear skies while the solid line is the nominal minimum irradiance ratio obscured overcast sky

regression of clear sky irradiances. The mean cloud optical depth varied from 6 to 10 (Table 1) with a typical standard deviation (SD) of 11 for a given 10° solar zenith angle class. These cloud optical depths were comparable to the mean thickness in 1984 for this latitude (12; Tselioudis et al., 1992). The range in irradiance ratio was relatively constant across the range of solar zenith angles used in this study (Fig. 3B), indicating that even though direct beam irradiance was present at the time of observations, the diffuse irradiance dominated the global irradiance. In addition, the height of the cloud base did not correlate with the irradiance ratio, in contrast with the conclusions of Nunez et al. (1994).

A total of 791 values were used in the *N-UVA* analysis while only 496 values were used in the *N-UVB* analysis. The low number of UVB values available for analysis were due to the exclusion criteria for quality control described previously. The SD of the UVA and UVB datasets were 0.087 and 0.099 with corresponding skewness of 1.49 and 3.57. The coefficient of variation (CV) of N_m-*UVA* for the translucent overcast sky was 27%. The corresponding CV of N_m-*UVB* was 33%.

3.1 Measured Sky Radiance Distribution

As with the clear sky UV radiance distributions (Grant et al., 1996a), N_m was not uniformly distributed throughout the sky hemisphere. The N_m were typically symmetrical about the principal plane of the sun (Fig. 4). The translucent overcast sky N_m-*UVA* and -*UVB* distributions were similar to each other, although the UVB distributions typically had less pattern and greater variability across the sky (Fig. 4). The general characteristics of the N_m distributions corresponded with the measurements in the entire short-wave of Coombes and Harrison (1988) and in the photosynthetically-active waveband of Grant et al. (1996b). No region of reduced radiance opposite to the solar disk was found in the translucent overcast distributions as was evident in the clear sky radiance distributions (Grant et al., 1996a). This is presumably

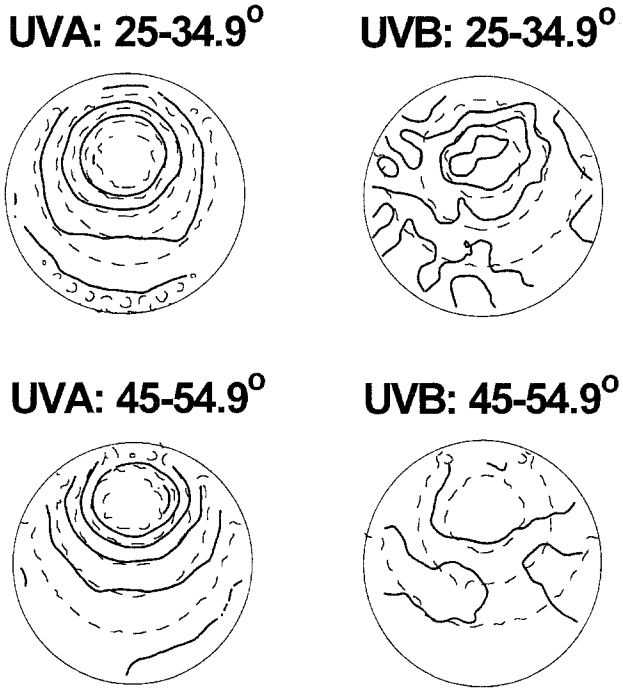

Fig. 4. N_m -UVA and N_m -UVB for two solar zenith angle classes. The title over each plot represents the waveband and range in solar zenith angles included in the sky radiance map. The solid and dashed lines represent isopleths of measured and modeled normalized radiance respectively. The isopleth interval is $0.05/\pi$ Sr

due to the greater multiple scattering in the translucent overcast sky than the clear sky. The apparent increase in sky radiance as the sky zenith approaches the horizon, termed 'horizon brightening' was evident in the UVA distributions at high solar zenith angles (Fig. 4) as it was under clear sky conditions (Grant et al., 1996a).

The sky radiance of an overcast sky is commonly assumed to be isotropically distributed in the sky. This assumes that the radiance distribution is purely a result of multiple-scattering. Were the uniform overcast sky (UOC) model applicable, a mean radiance of $1/\pi\ \pi \mathrm{Sr}^{-1}$ would fit the N_m. For the UOC model, the model RMSE is equal to the N_m SD. This RMSE was used as a baseline for determining improvements in modeling the sky radiance. The mean overcast sky N_m-*UVB* was lower than that of the N_m-*UVA*, in part because the N_m-*UVA* is more clearly influenced by the circumsolar radiation (Fig. 5).

A large proportion of the N_m distribution can be accounted for by a single scattering event represented by the circumsolar scattering angle Ψ. Figure 5 illustrates the influence of Ψ (Eq. (3b)) on the N_m. Note a basic negative exponential relationship between Ψ and N_m in both wavebands with greater decline in N_m with increasing Ψ for the UVA waveband than the UVB wave-band (Fig. 5). The reduced influence of Ψ on the normalized radiance distributions in the UVB corresponded with expected influence of multiple scattering events on the radiance distribution.

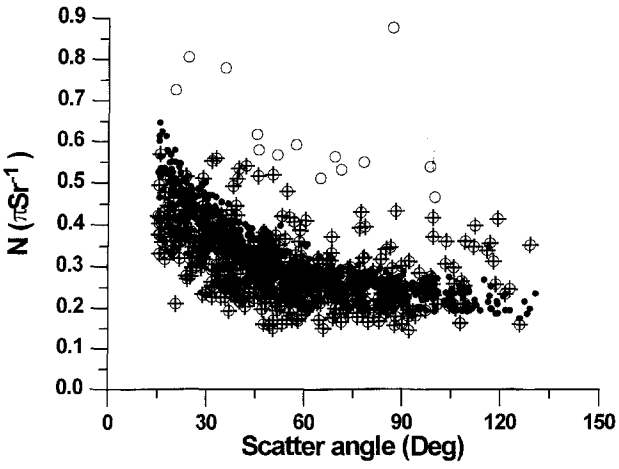

Fig. 5. Variation of N_m -UVA and N_m -UVB with respect to scatter angle. The closed circles represent the N_m UVA while the open circles and circles with crosses represent the N_m UVB. The circles with crosses represent the N_m UVB that passed the skewness test for outliers in the modeled N as described in the text

3.2 *Sky Radiance Distribution Modeling*

The translucent overcast N_m-*UVA* and -*UVB* were modeled by equations of the form of Eq. (3a) and Eq. (4). The application of the SOC sky distribution (Eq. (4)) to N_m for the translucent overcast sky conditions resulted in RMSE greater than the SD of the N_m. The lack of fit of the translucent overcast sky measurements to Eq. (4) is clear when one considers the assumption of N_m variability with respect to scatter angle (Fig. 5) and hence also solar zenith angle, while SOC assumes variability only with respect to zenith angle.

Prior to filtering the datasets of outliers, the best fit of the translucent overcast sky N_m-*UVA* and N_m-*UVB* to Eq. (3a) resulted in a coefficient of determination (r^2) of 0.62 for the UVA waveband and 0.08 for the UVB waveband. An analysis of the multiple scattering component of the best fit of Eq. (3a) yielded values of 0.136 for the UVA, 0.167 for the UVB, 0.105 for the PAR (based on Grant et al., 1996b), and 0.241 for the SW (based on Coombes and Harrison, 1988). The progression of increasing values from PAR to UVA to UVB corresponds with radiation theory. The high level of the SW estimate is probably a result of Coombes and Harrison (1988) choosing a different minimum scatter angle for model validation measurements.

Horizon brightening, as approximated by the third term of Eq. (3a), decreased with decreasing waveband in the order of SW, PAR, UVA, and UVB (Table 2). This corresponded with radiation theory that indicates horizon brightening is a function of surface albedo enhancing multiple scattering. The ground albedo in the UVA and UVB is typically less than 3% (Feister and Grewe, 1995; Blumthaler and Ambach, 1988) while that in the PAR are typically 5% (Feister and Grewe, 1995) and in the SW 25% (Iqbal, 1983). Evidence of the horizon brightening in the *N-UVA* radiance distributions can be seen in Fig. 4. No evident brightening existed in the *N-UVB*.

The overall circumsolar influence of forward-scattered radiation on N_m-*UVA* and N_m-*UVB* was estimated by assuming a set of conditions ($\Psi = 15°$, $\Theta^* = 30°$ and $\Theta = 45°$) and evaluat-

ing the last term in Eq. (3a). Results of this approximation showed the circumsolar influence to be greater for the UVA than the UVB (0.22 and 0.16 respectively) wavebands. The corresponding values for the PAR (from Grant et al., 1996b) and SW (from Coombes and Harrison, 1988) wavebands were estimated as 0.34 and 0.14 respectively. The relative circumsolar influence decreasing from PAR to UVA to UVB agrees with radiation theory. The low value for the SW is not consistent with the other wavebands or radiation theory. A comparison across all wavebands of the slope of the circumsolar region with increasing Ψ (m in Eq. (3a)) shows that the slope is not wavelength dependent (within 10%, Table 2). This conclusion is in contrast to N_m-*UVA* and N_m-*UVB* (Fig. 5), suggesting that the model of Eq. (3a) does not account for all factors in the N_m variability.

Evaluation of the UVA model residuals showed that the poorest modeling occurred when Ψ was small (Fig. 6A), with the greatest errors

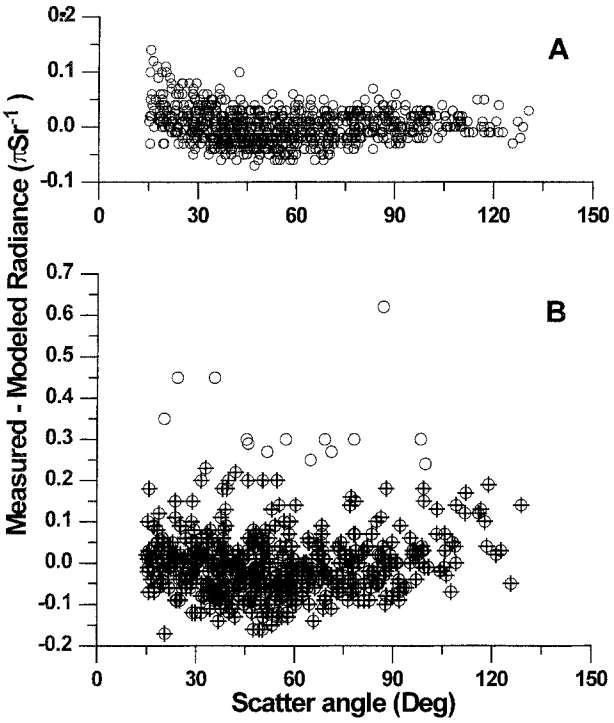

Fig. 6. Residual analysis of the UV overcast sky radiance functions. Panel A illustrates the residual of the UVA model (measured-modeled values) to the N_m-UVA. Panel B illustrates the residual of the UVB model to the N_m-UVB where the circled crosses represent the data that passed the skewness outlier test, while the circles alone represent the data that is excluded as a result of the skewness outlier test for outliers

when Ψ was less than 30° (corresponding to the high N_m values.) The low r^2 value of the UVB model based on Eq. (3a) was largely due to the great 'near random' variability evident in the model residuals and probably due to the low signal to noise ratio of the sensor (Fig. 6B). This variability may in part be due to scattering off the sides of clouds, but it is believed that the very large *N-UVB* were due to signal noise problems and not sky radiance variability. The measured *N-UVB* and *N-UVA* were tested for outlier values on the assumption that the extreme outliers were due to noise. After application of the skewness test for outliers (ASTM, 1980), the UVB dataset was reduced by 14 values, reducing the SD of the residual (model RMSE) from 0.091 to 0.070 and the skewness from 1.96 to 0.73. Inspection shows that the deleted values are indeed extreme values in the dataset (values indicated by the open circle in Figs. 5 and 6B). Model fit to the reduced *N-UVB* data set increased the model bias from 0.002 to 0.008. The corresponding r^2 value for the final evaluation of the *N-UVB* model was 0.25. No N_m-*UVA* were excluded from the final model evaluation as a result of the outlier test.

4. Summary and Conclusions

The overcast sky radiance in the UVA and UVB wavelength bands were measured during the summer of 1993 and modeled using various radiance distribution functions. The UVB irradiance ratio (overcast sky irradiance/clear sky irradiance estimate) under overcast skies was not dependent on the height of the cloud base, the opaque cloud fraction, or the solar zenith angle. Consequently, the diffuse sky radiance evidently dominates the global UVB irradiance and be relatively unaffected by the variable scattering off opaque clouds.

The translucent overcast normalized sky radiance distributions (units of πSr^{-1}) were modeled according to the Coombes and Harrison formulation (Eq. (3a)). as:

$$N_{UVA} = 0.120 + 0.032\Theta + 0.064\cos\Theta^* + 0.361e^{-1.9\Psi}$$

and

$$N_{UVB} = 0.152 + 0.029\Theta + 0.029\cos\Theta^* + 0.247e^{-1.7\Psi}$$

with final r^2 values of 0.62 and 0.25 for the UVA and UVB respectively.

The actual sky radiance distribution can be estimated using the above functions for N as: $N_a(\Theta, \Phi) = \hat{I}_{\text{diff}} N(\Theta, \Phi)$. The distributions developed here provide a means of describing the overcast sky radiance distributions in the UVB and UVA wavebands over natural surfaces. Additional measurements of the UVB sky radiance distribution (using improved signal shielding and conditioning) under translucent overcast conditions are needed to strengthen the model fit as well as verify that UVB irradiance under these skies do not in fact exceed that under clear skies with the same ozone column thickness.

Acknowledgments

The authors thank Thomas Sperback for his help in collecting and processing the radiance measurements. This research was funded in part by the USDA Forest Service Northern Global Change Research Program under cooperative agreement 23-793 of the Northeastern Forest Experiment Station. Thanks also go to the Institut für Meteorologie and Physik, Universität für Bodenkultur, Vienna, Austria for providing support during the analysis. This is journal paper no. 15211 of the Purdue Experiment Station.

References

ASTM., 1980: Standard practice for dealing with outlying observations. American Standards of Testing and Materials. *Standard,* E1 78-80.

Beaglehole, D., Carter, G. G., 1992: Antarctic skies. 2. Characterization of intensity and polarization of skylight in a high albedo environment. *J. Geophys. Res.*, **97**, 2597–2600.

Blumthaler, M., Ambach, W., 1988: Solar UVB-albedo of various surfaces. *Photochem Photobiol.,* **48**, 85–88.

Blumthaler, M., Ambach, W., Salzgeber, M., 1994: Effects of cloudiness on global and diffuse UV irradiance in a high-mountain area. *Theor. Appl. Climatol.,* **50**, 23–30.

Brunger, A. P., Hooper, F. C., 1991: Measured short-wave sky radiance in an urban atmosphere. *Solar Energy,* **47**, 137–142.

Brunger, A. P., Hooper, F. C., 1993: Anisotropic sky radiance model based on narrow field of view measurements of short-wave radiance. *Solar Energy,* **51**, 53–64.

Coombes, C. A., Harrison, A.W., 1988: Angular distribution of overcast sky short wavelength radiance. *Solar Energy,* **40**, 161–166.

Deepak, A., 1977: Inversion of solar aureole measurements for determining aerosol characteristics. In: Deepak, A. (ed.) *Inversion Methods in Atmospheric Remote Sounding*. New York: Academic Press, pp. 265–291.

Draper, N., Smith, H., 1981: *Applied Regression Analysis*, 2nd edn. New York: Wiley 709p.

Feister, U., Grewe, R., 1995: Spectral albedo measurements in the UV and visible region over different types of surfaces. *Photochem. Photobiol.,* **62**, 736–744.

Ferguson, T. S., 1961: Rules for rejection of outliers. *Revue Inst. de Stat.,* **3**, 29–43.

Fritz, S., 1955: Illuminance and luminance under overcast skies. *J. Opt. Soc. Amer.,* **45**, 820–825.

Garrison, L. M., Murray, L. E., Doda, D. D., Green, A. E. S., 1978: Diffuse-direct ultraviolet ratios with a compact double monochronometer. *Applied Optics,* **17**, 827–836.

Grant, R. H., 1996: Characterization of UVA and UVB irradiance sensor systems, pp. 169–172 in *Proceedings of the 22nd Conf. on Agricultural and Forest Meteorology,* American Meteorological Society.

Grant, R. H., Heisler, G. M., Gao, W., 1996a: Clear sky radiance distributions in ultraviolet wavelength bands. *Theor. Appl. Climatology.* (in press).

Grant, R. H., Heisler, G. M., Gao, W., 1996b: Photosynthetically-active radiation: sky radiance distributions under clear and overcast conditions. *Agric. and Forest Meteorol.* (in press).

Green, A. E. S., Cross, K. R., Smith, L. A., 1980: Improved analytic characterization of ultraviolet skylight. *Photochem. Photobiol.,* **31**, 59–65.

Green, A. E. S., Swada, T., Shettle, E. P., 1974: The middle ultraviolet reaching the ground. *Photochem. Photobiol.,* **19**, 251–259.

Iqbal, M., 1983: *An Introduction to Solar Radiation.* Toronto, Canada: Academic Press, 390 pp.

Kittler, R., Valko, P., 1993: Radiance distribution on densely overcast skies: comparison with CIE luminance distribution. *Solar Energy,* **51**, 349–355.

Madronich, S., DeGruijl, F. R., 1994: Stratospheric ozone depletion between 1979 and 1992: implications for biologically active ultraviolet-B radiation and non-melanoma skin cancer incidence. *Photochem. Photobiol.,* **59**, 541–546.

Nack, M. L., Green, A. E. S., 1974: Influence of clouds, haze, and smog on the middle ultraviolet reaching the ground. *Appl. Optics,* **13**, 2405–2415.

Nunez, M., Forgan, B., Roy, C., 1994: Estimating ultraviolet radiation at the earth's surface. *Int. J. Biometeorol.,* **38**, 5–17.

Powkrowski, G. I., 1929: Über einen scheinbaren Mie-Effect und seine mögliche Rolle in der Atmosphärenoptik, *Zeitschrift für Physik,* **53**, 67–71.

Rosen, M. A., 1992: Investigation of the validity of the TDRC model for the distribution of diffuse sky radiance. *Solar Energy,* **48**, 123–131.

Schippnick, P. F., Green, A. E. S., 1982: Analytical characterization of spectral irradiance in the middle ultraviolet. *Photochem. Photobiol.,* **35**, 89–101.

Spinhirne, J. D., Green, A. E. S., 1978: Calculation of relative influence of cloud layers on received ultraviolet and integrated solar radiation. *Atmos. Environ.,* **12**, 2449–2454.

Stamnes, K., Slusser, J., Bowen, M., 1991: Derivation of total ozone abundance and cloud effects from spectral irradiance measurements. *Appl. Optics,* **30**, 4418–4426.

Steven, M. D., Unsworth, M. H., 1980: The angular distribution and interception of diffuse solar radiation below overcast skies. *Quart. J. Roy. Meteor. Soc.,* **106**, 57–61.

Tselioudis, G., Rossow, W. B., Rind, D., 1992: Global patterns of cloud optical thickness variation with temperature. *J. Climate,* **5**, 1484–1495.

Authors' addresses: Richard H. Grant and W. Gao, Department of Agronomy, Purdue University, W. Lafayette, IN 47907-1150, U.S.A.; Gordon M. Heisler, USDA Forest Service, Northeastern Forest Experiment Station, SUNY-CESF, Syracuse, NY, 13210, U.S.A.